Original Research

Investigating the Effect of Cobalt Ions on the Optical and Structural Properties of Zinc Ferrite Synthesized by the Sol-Gel Technique

Ahmed Hamed Abed [1], Nazar Khalaf Mahan [2], Hussein Subhi Abdulrahman [1], Tagreed M. Al-Saadi [3,*]

[1] The General Directorate for Education in Diyala, Baqubah 32001, Diyala, Iraq;
[2] Department of Physics, College of Science, Mustansiriyah University, Baghdad 10071, Iraq;
[3] College of Education for Pure Science, Ibn Al Haitham, University of Baghdad, Baghdad 10071, Iraq
* Correspondence: taghreed.m.m@ihcoedu.uobaghdad.edu.iq

Received: December 9th, 2025; Accepted: February 9th, 2026

Abstract: Zinc ferrite with composition ($Zn_{1-x}Co_xFe_2O_4$) (x = 0, 0.3, 0.4, 0.5, and 0.6) has been prepared using the sol-gel technique. The samples prepared were characterized using X-ray diffractometry (XRD) and transmission electron microscopy (TEM) techniques. The nanocrystallites have been found to have a size range of 63.023–99.036 nm. The optical properties for all samples' absorbance and energy band gap (Eg) were measured by the design of Tauc's diagram. The indirect and (direct) optical band gaps of the synthesized ($Zn_{1-x}Co_xFe_2O_4$) ferrite increased from 2.65 eV to 3.40 eV and 4.07 eV to 4.60 eV with increasing the doping percentage of Co as x = 0–0.6. The increase in energy gaps (Eg) value with Co ions doping is possible because of sub-bandgap energy level formation.

Keywords: zinc ferrite; nanoparticles; optical properties; Williamson-Hall; XRD; TEM

1. Introduction

The properties of crystalline spinel ferrites at the nano- and sub-nanoscale are heavily dependent on their synthesis pathway, chemical composition, and cation distribution in the crystal lattice [1]. Spinel ferrites are ferrimagnetic semiconducting metal oxides made using a general formula MFe_2O_4, where M is a divalent metal ion. Their ferrimagnetic response occurs based upon the unequal magnitude antiparallel magnetic moments at tetrahedral (A) and octahedral (B) sites, producing spontaneous magnetization in the absence of an external magnetic field [2,3].

Due to the high electrical resistivity, low dielectric losses, strong mechanical stability, and high magnetic permeability, spinel ferrites have drawn much study for applications such as electronics, energy conversion, and electromagnetic devices [4,5]. Of spinel ferrites, cobalt ferrite ($CoFe_2O_4$) and zinc ferrite ($ZnFe_2O_4$) are the two most prominent end members that have a unique distribution of cations and physical properties [6,7]. Cobalt ferrite typically crystallizes in an inverse spinel where Co^{2+} ions dominate the octahedral (B) regions and Fe^{3+} ions are scattered between both the locations of the A and B sites. By contrast, zinc ferrite possesses a normal spinel structure, where Zn^{2+} ions are concentrated at the tetrahedral (A) sites, and Fe^{3+} ions take place in the octahedral (B). Such differences in cation conformation are essential for the structural, magnetic, electrical, and optical properties of ferrite materials [8,9].

Ferrimagnetic spinel ferrites are represented by the chemical formula $A^{2+}B_2^{3+}O_4$, where A denotes divalent metal ions such as Zn^{2+}, Co^{2+}, Ni^{2+}, Mn^{2+}, or Mg^{2+}, and B signifies trivalent ions like Fe^{3+}. The substitution of metal ions at specific crystallographic sites is a prevalent technique for modifying the physicochemical properties of ferrite nanoparticles [10]. Such ionic substitution would produce lattice distortion, change the size of the crystal, affect the concentration of cation distribution, and therefore can lead to changes in the electronic band structure and the optical response of a material [11,12]. Spinel ferrite films have attracted special attention in optical and optoelectronic applications in the past few years owing to semiconducting properties and adjustable energy band gaps. These materials exhibit robust optical properties, largely because many structural parameters, such as lattice strain, crystallite size and defect concentration, are controlled through selective doping [13]. Alterations in the composition and concentration of the substituted metal ions can considerably alter the density of electronic states and transition probabilities of the electronic states and thus the optical absorption behavior and band gap energy, significantly different. It is, therefore, believed that doped spinel ferrites are flexible for band gap design, and therefore are promising materials for various applications in photocatalysis, UV-responsive devices and optoelectronic systems [14,15].

Although there have been numerous studies focusing on Co-doped zinc ferrites, there is a lack of clear knowledge regarding the interaction of the high levels of cobalt replacement on the structural parameters and on the evolution of optical band gap, especially for materials prepared by the sol–gel method. While numerous previous investigations have concentrated on low doping concentrations or highlighted the magnetic behavior of the materials, systematic studies correlating the structural elements to optical properties over a larger Co substitution range are still rare. This is a critical research gap that drives the current study. In spite of different factors of the crystallization method, this work seeks to investigate the effects of Zn^{2+} ion substitution, in which Co^{2+} ion is substituted within the span of 0 to 0.6, of zinc ferrite ($Zn_{1-x}Co_xFe_2O_4$), synthesized with sol–gel method. Particular focus is given to the impact of cobalt incorporation on the structural and optical properties of the ferrite system as a means of elucidating the composition–structure–property mechanism and evaluating the possible properties of Co-doped $ZnFe_2O_4$ for advanced optical applications.

2. Experimental Method

The preparation Cobalt substituted zinc ferrite process is done by Auto combustion method mixing metal nitrates as cobalt nitrate ($Co(NO_3)_2.6H_2O$), zinc nitrate ($Zn(NO_3)_2.6H_2O$), iron nitrate ($Fe(NO_3)_3.9H_2O$) and one mole of citric acid monohydrate ($C_6H_8O_7.H_2O$). were dissolved in distilled water. After that, Ammonia was added to the prepared solution to adjust the pH value to (7) .Mix the solution in a heat-resistant beaker using a magnetic stirrer for (50 min) at room temperature to ensure complete homogeneity of the solution. We noticed the formation of a high-viscosity gel after intense stirring and evaporation at (100 °C). Then, the resulting gel was heated at a temperature of (250 °C). The gel underwent self-combustion, forming a xerogel. The resulting powder was placed in a high-heat resistant porcelain bowl, then placed inside an oven for calcination at a temperature of (900 °C) for two hours to get rid of impurities resulting from the annealing process (carbon oxide) and water residue, thus completing the preparation of ($Zn_{1-x}Co_xFe_2O_4$) powder. The calcination temperature of 900 °C was selected to ensure complete decomposition of the xerogel precursor and formation of a well-crystallized single-phase spinel structure. Lower temperatures resulted in poor crystallinity, while higher temperatures may cause excessive grain growth. The increase in crystallite size with Co content is discussed in terms of enhanced diffusion and grain coalescence at high temperature.

3. Results and Discussion

3.1. X-ray Diffraction

X-ray powder diffraction characteristics of the synthetic (x = 0, 0.3, 0.4, 0.5 and 0.6) samples were shown in Figure 1(a). It shows the X-ray diffraction results for samples broad profile prominent peaks which correspond to (111), (220), (311), (222), (400), (422), (511), (440), (620), (533), (622), (444), (642) and (731) lattice plane reflection [16]. The diffraction peak positions were completely matched with single phase ($Zn_{1-x}Co_xFe_2O_4$) without any secondary phase profile given in powder diffraction file (PDF) No. 89-1012 [17]. The impact of substituting Fe^{+3} for Co^{+3} on the physical and chemical properties of Co-Zn ferrite is among the most prevalent substitutions that do not alter the cubic Fd3m spinel structure. Moreover, we noticed a change in the intensity of the peaks, especially the peak (311), where its intensity decreased with increasing doping ratios and a full width at half maximum (FWHM). This indicates that the crystal structure is affected by the process of replacing the Zn ion with a Co ion, whereby the normal spin structure is transformed into an inverse spinel structure while maintaining the face-centered cubic (FCC) crystal structure [18].

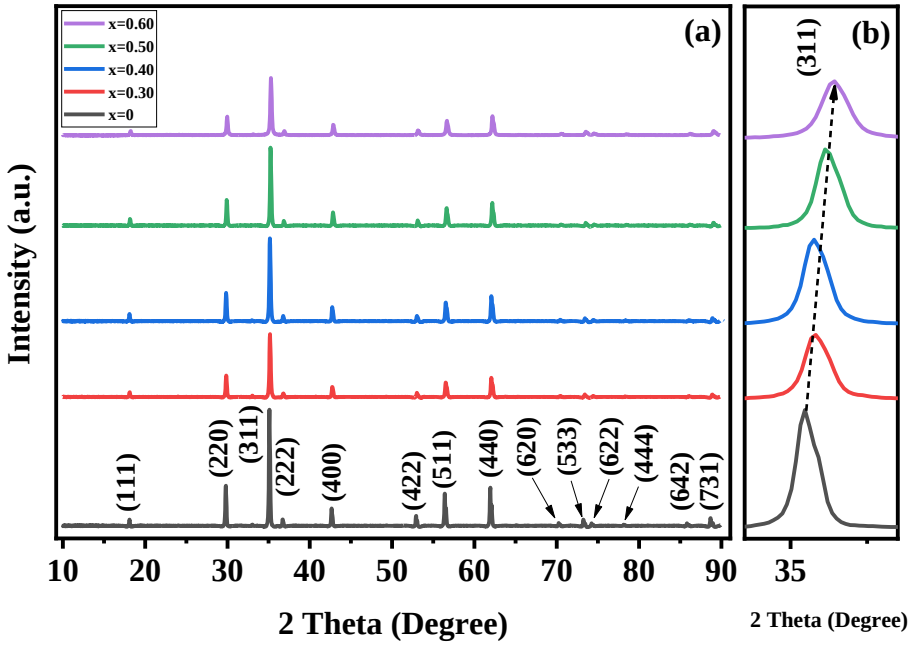

Figure 1. X-ray diffraction patterns of ($Zn1-_xCo_xFe_2O_4$) for all samples (x = 0, 0.3, 0.4, 0.5 and 0.6). (a) Full pattern; (b) (311) peak.

Figure 1(b) reveals the position of the X-ray diffraction peak has been observed to be shifted towards a higher angle for a sample (x = 0.4, 0.5, 0.6).

In this case, zinc ionic radii (0.64 Å), which is less than the 0.66 Å cobalt ionic radii. The X-ray diffraction peak may shift towards a higher angle that is contradictory for samples (x = 0, 0.3) or the cobalt ionic Co or zinc ionic is present in more than one valence state, depending on the difference in the values of the ionic radii. This shows that the lattice shrinks as the Co concentration rises [19,20].

3.2. Crystallite Size, Lattice Parameter, Dislocation Density, and Micro-Strain Analysis

The broadening of X-ray diffraction peaks indicates the presence of numerous measures, including micro-strain, wavelength selection, instrumental broadening, and crystallite size. Using a Williamson-Hall (W–H) Equation (1) for calculating average crystallite size from the full width half maxima of an X-Ray diffraction peak [21,22].

$$\beta_{hkl} = \left(\frac{K\lambda}{D}\right) + 4\varepsilon \sin\theta \tag{1}$$

where K is the shape factor (~0.94), λ is the X-ray's wavelength of Cu Kα radiation, β is the XRD peak's full width at half maximum (FWHM), and θ is the Bragg angle, (ε) micro-strain.

Using "fullprof" software, the lattice constant was calculated of $Co_xZn_{1-x}Fe_2O_4$ for the prominent peak (311) using the following equation [23].

$$a = d\sqrt{h^2 + k^2 + l^2} \tag{2}$$

where (hkl) is Miller indices and (d) is the perpendicular distance between two adjacent planes in the crystal. The quality of the samples is estimated by calculating the dislocation density (δ) using the relation [24,25].

$$\delta = \frac{1}{D^2} \tag{3}$$

Table 1. The calculated values of the lattice parameter a (Å), the crystallite size (D), the dislocation density (δ), the micro-strain (ε), and the lattice parameter (a) of Zn ferrite systems.

Composition	a (Å)	ε × 10^{-3}	δ × 10^{-3} Line /cm^2	D (nm)
$ZnFe_2O_4$	8.4741	–0.3	0.25	63.023
$Zn_{0.7}Co_{0.3}Fe_2O_4$	8.4766	–0.07	0.20	69.325
$Zn_{0.6}Co_{0.4}Fe_2O_4$	8.4882	0.2	0.16	77.028
$Zn_{0.5}Co_{0.5}Fe_2O_4$	8.4915	0.4	0.13	86.656
$Zn_{0.4}Co_{0.6}Fe_2O_4$	8.5022	0.5	0.10	99.036

Table 1 clearly shows the increase of the Co doping ratio from x = 0 to x = 0.6 increasing the strain values from 0.3 × 10^{-3} to 0.5 × 10^{-3} and increasing the size of crystallites from 63.023 nm to 99.036 nm. Thus, an inverse relationship between the micro-strain (ε) exists and crystallite size (D) show that the dislocation density (δ) decreases with increasing Co ionic doping. This is explained by the fact that co-doping has improved the crystallization process. The increase in the crystallite size (D) leads to a decrease in the dislocation density (δ) and a decrease in micro-strain (ε), as shown in Table [26].

Figure 2 represents Williamson–Hall plots for the Nanoparticle size of the two samples with x = 0 and x = 0.3 showed negative micro-strain, which may be due to lattice shrinkage [27]. When Co^{2+} ions are doped at the Zn site, a positive micro-strain is introduced. This micro-strain increases as the concentration of Co^{2+} ions (x) increases because of the larger crystallites [28]. Lattice parameter a (Å) was found to increase with cobalt concentration and this may be because of the biggest ionic radius of the cobalt ion [29].

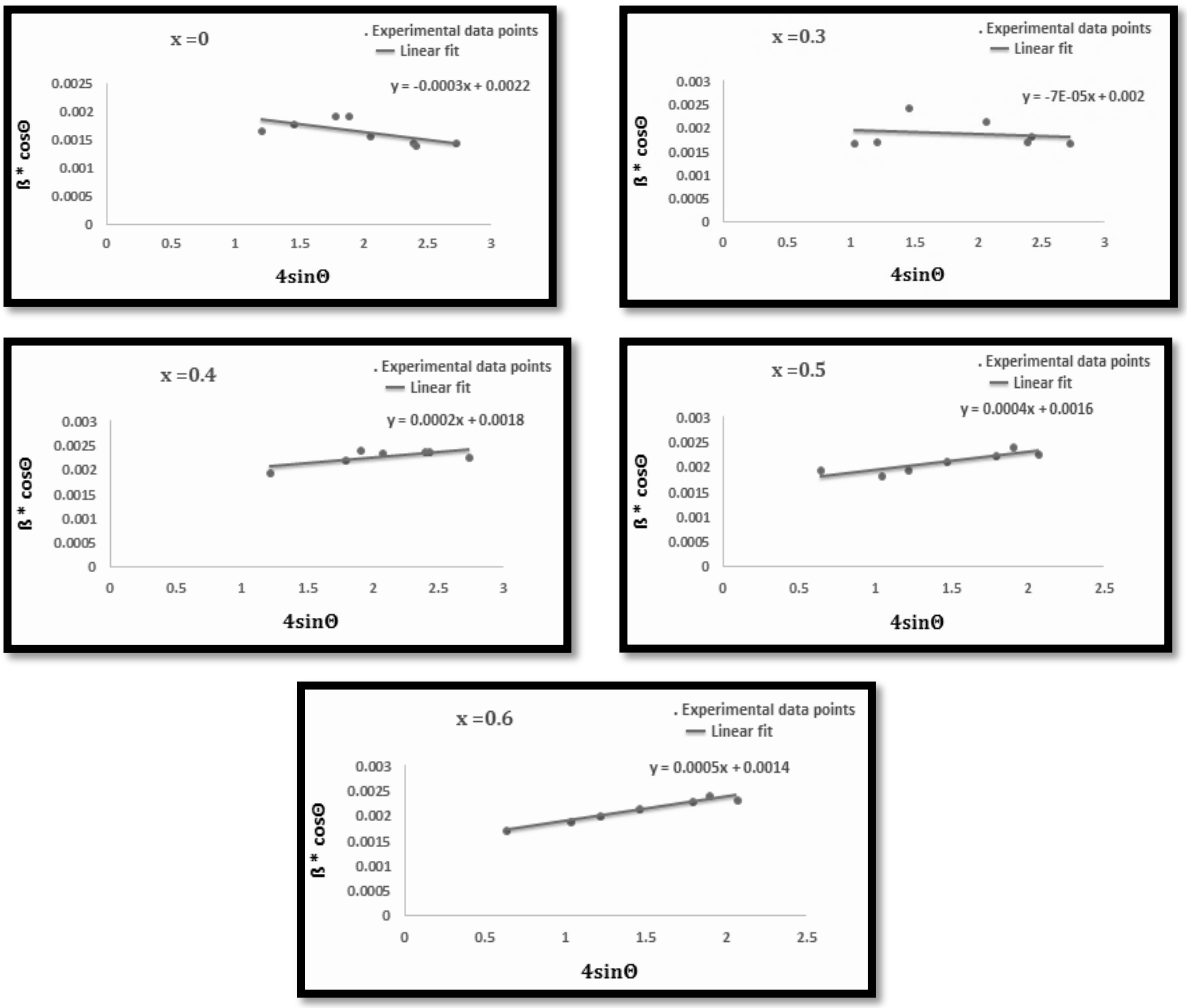

Figure 2. The Williamson–Hall (W–H) plots for the present $Co_xZn_{1-x}Fe_2O_4$ ferrite (x = 0, 0.3, 0.4, 0.5 and 0.6).

3.3. TEM Analysis

Figure 3 shows the TEM images of the ferrite structure $Zn_{1-x}Co_xFe_2O_4$ nano ferrites. The agglomeration of the nano ferrite particles at a wide scale is observed. The particle agglomeration is linked to high-temperature calcination and magnetic dipole–dipole interactions. The agglomeration is attributed to sintering effects at 900 °C and increased interparticle attraction with increasing Co concentration [30]. An average particle size ranging from 54.84 to 84.07 nm is observed by the TEM images. The particle size measurement of $Zn_{1-x}Co_xFe_2O_4$ using X-ray diffraction analysis was found to be larger than that with TEM measurement.

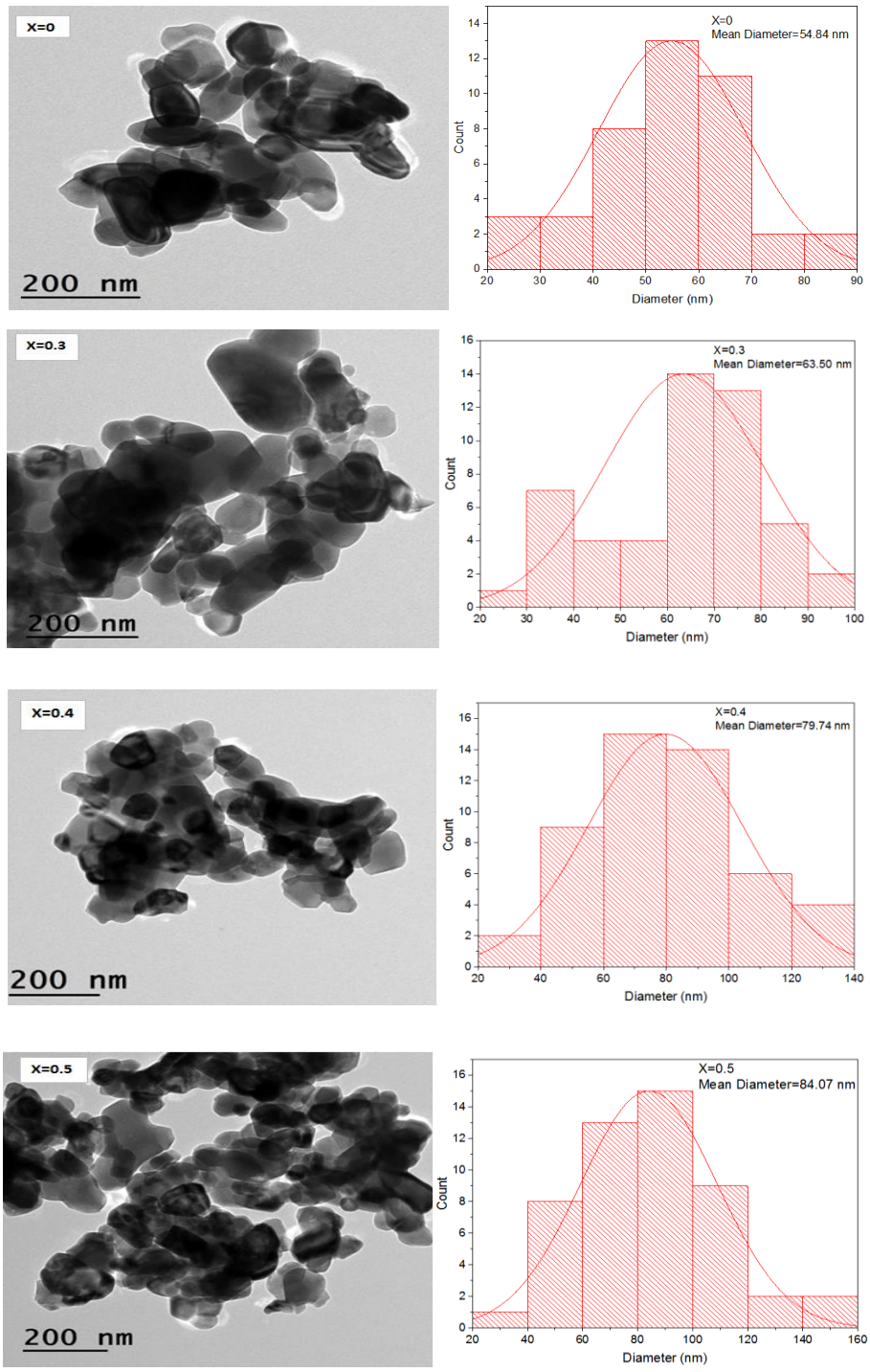
X=0
200 nm
X=0
Mean Diameter=54.84 nm
Count
Diameter (nm)
X=0.3
200 nm
X=0.3
Mean Diameter=63.50 nm
Count
Diameter (nm)
X=0.4
200 nm
X=0.4
Mean Diameter=79.74 nm
Count
Diameter (nm)
X=0.5
200 nm
X=0.5
Mean Diameter=84.07 nm
Count
Diameter (nm)

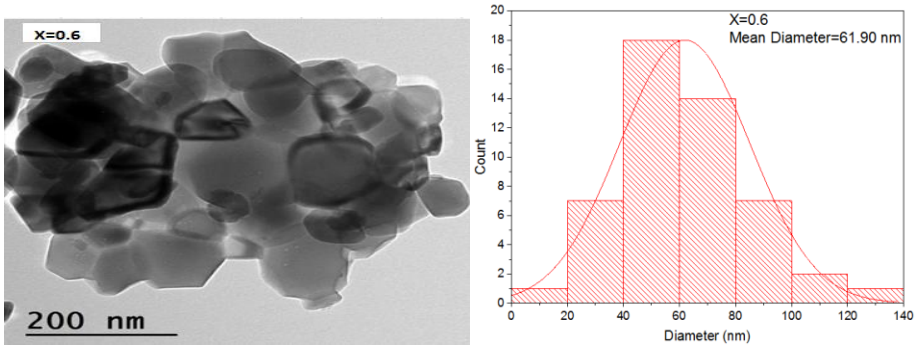

Figure 3. TEM images and size distributions of $Co_xZn_{1-x}Fe_2O_4$ nano ferrite (x = 0, 0.3, 0.4, 0.5 and 0.6). The scale bar shown in the TEM images represents 200 nm.

3.4. Optical Properties

The optical characteristics are very important in the ferrites through which the fields of several can be determined. Figure 4 shows the variation that the optical absorbance spectra of Co-substituted Zn ferrites as a function of wavelength (nm) [31], i.e., the absorbance decreases as the Co doping increases the maximum at x = 0, but decreases for all samples (x = 0.3, 0.4, 0.5, 0.6) [32]. The desired band gaps for all samples can be calculated from Tauc's equation [33].

$$\alpha hv = A\,(hv - Eg)^{n} \tag{4}$$

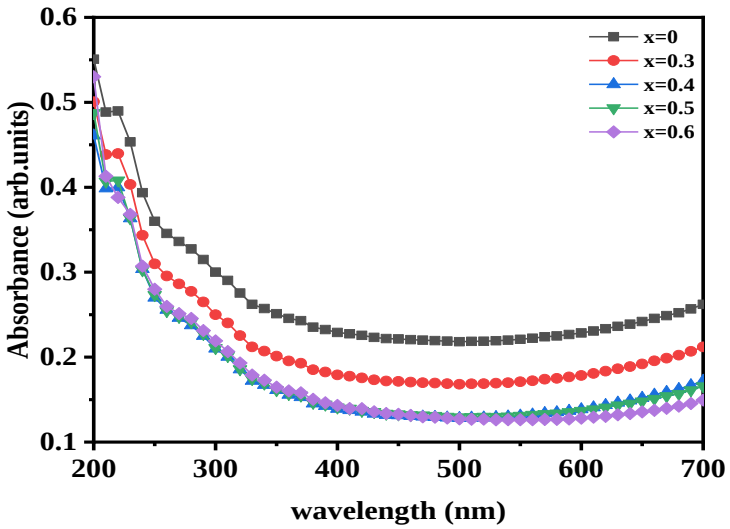

Figure 4. UV–visible absorbance spectra of $Zn_{1-x}Co_xFe_2O_4$ nanoparticles.

Here, (Eg) stands for optical band gap, (α) for coefficient of absorption, (n) 2 or ½ for indirect or direct energy band gap for hexaferrite material, (A) for a constant dependent on the transition probability, and (hv) for photon energy. (α) The coefficient of absorption can be obtained using this relation [34].

$$\alpha = \frac{4\pi k}{\lambda} \tag{5}$$

where k is the absorption index and λ is the wavelength (nm).

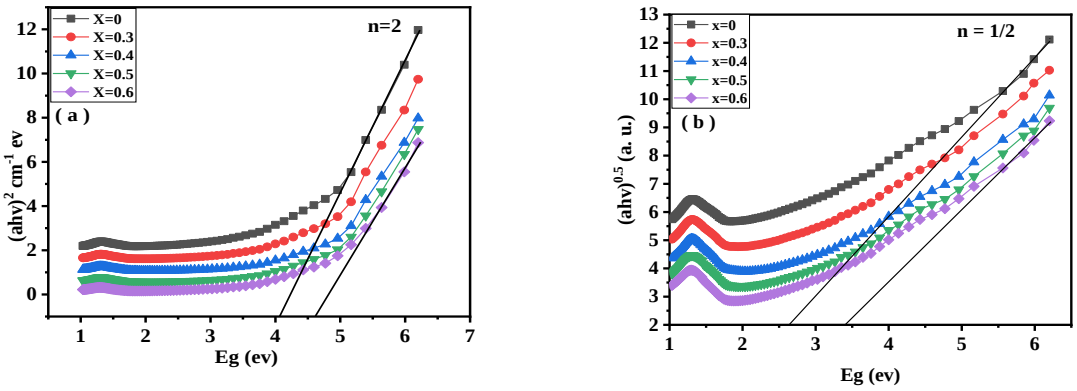

Figure 5. Tauc's plots optical band gap determination of $Zn_{1-x}Co_xFe_2O_4$ nanoferrites for (a) direct (n = 2) and (b) indirect (n = 1/2) allowed transitions.

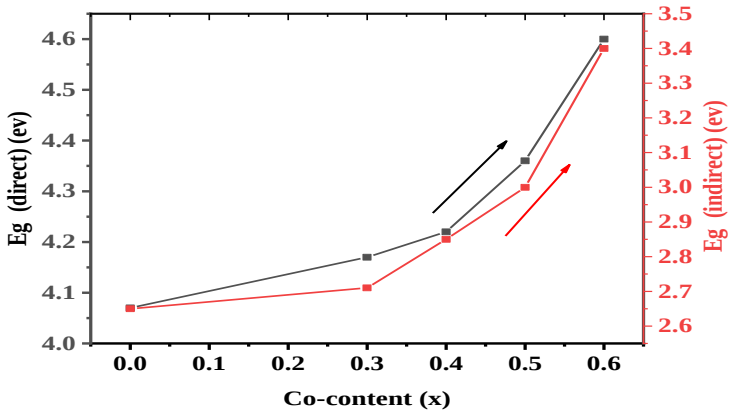

Figure 6. The Co-content dependence of the estimated indirect and direct energy gaps.

Optical investigations of the $Zn_{1-x}Co_xFe_2O_4$ combination (x = 0–0.6) demonstrate a distinct alteration in both the absorption spectra and the optical gap threshold with increasing cobalt concentration, indicating the profound structural and electronic influence of Co^{2+} doping on the ferrite's spin configuration. Initially, absorption spectra within the 200–700 nm wavelength range indicated that all samples demonstrated significant absorption in the ultraviolet area, which then diminished towards the visible spectrum. The undoped sample was found to have the highest absorption, while absorption values gradually decreased with increasing doping, indicating a redshift in the absorption curve towards higher wavelengths. This behavior is attributed to modifications in the energy levels resulting from the introduction of Co^{2+}, which carries d electrons capable of rearranging electron beams and reducing the density of states available for electron transitions in the shortwave region [35,36] as shown in Figure 4.

To better understand these changes, the energy gap was analyzed using Tauc diagrams for both direct and indirect allowed transitions as shown in Figure 5. These curves showed that the linear part of the relationship between $(\alpha h\nu)^n$ and $h\nu$ shifts uniformly with increasing cobalt content, indicating a significant change in the material's electronic structure. The direct energy gap showed a general decrease in light doping, while high doping ($x \geq 0.5$) showed a greater change in the slope of the lines, indicating a cumulative effect of cobalt in narrowing the valence and conduction bands. The indirect gap exhibited similar behavior with slightly lower values than the direct gap, which is expected due to the spin nature

of ferrite and the phonon-dependent electronic transitions. The robustness of this change in both the direct and indirect Eg reflects the redistribution of cations between tetragonal and octahedral crystalline sites, leading to a modification in the energy range of the electron bands [37,38].

The picture becomes clearer when examining the relationship between Eg values and the cobalt content (x). Figure 6 shows a clear upward trend in the optical gap with increasing doping. This behavior indicates that the introduction of Co^{2+} reduces structural defects and localized electronic states at higher concentrations, resulting in more ordered electron beams and widening, rather than narrowing, the optical gap. Samples at $x \geq 0.5$ also exhibit a sharp increase in Eg, suggesting gradual structural modifications within the spin lattice that contribute to raising the energy required for electron transitions. This aligns perfectly with the observed decrease in absorption at shorter wavelengths in the first curves [39,40]. In general, the increase in the optical band gap with Co doping is attributed to the combined effects of increased crystallite size, modification of lattice strain, reduced defect density, and changes in cation distribution between tetrahedral and octahedral sites, which alter the electronic band structure and transition probabilities [41].

Overall, the integrated analysis of the three figures clearly demonstrates that cobalt doping of $ZnFe_2O_4$ is an effective tool for tuning its optical properties through its direct influence on the electronic structure and cation arrangement within the spin lattice. Doping leads to a decrease in absorption in the ultraviolet region, a regular change in Tauc curves, and a gradual increase in Eg values with increasing x, making this material a suitable candidate for applications that require a wide optical gap and low absorption in the visible region, such as photovoltaic and photoelectric materials and catalysts under UV irradiation [42].

4. Conclusions

Zinc ferrite ($Co_xZn_{1-x}Fe_2O_4$) nanoparticles were successfully prepared using the sol-gel method. The effect of Co ions on the structural and optical parameters was investigated, and crystallite size was observed in the range of 63.023 to 99.036 nm, revealed by X-ray diffraction, which is comparable with the particle sizes observed in SEM images. Lattice parameter (a) was found to increase with cobalt concentration, and this may be because of the larger ionic radius of the cobalt ion. Moreover, we noticed a change in the intensity of the peaks, especially the peak (311), where its intensity decreased with increasing doping ratios and a widening in the peak width (FWHM). This indicates that the crystal structure is affected by the process of replacing the Zn ion with a Co ion, whereby the normal spin structure is transformed into an inverse spinel structure while maintaining the ferrites are materials that have a magnetic moment spontaneously and face-centered cubic (FCC) crystal structure. A gradual increase in the optical energy gap and decrease in absorbance spectra imply sub-bandgap energy level formation; UV-vis absorbance measurements have not observed any differences in structural composition due to the Co substitution.

Acknowledgments: Not applicable.

Availability of Data and Materials: The datasets used and / or analyzed during the current study are available from the corresponding author upon reasonable request.

Funding: This research received no external funding.

Author Contributions: Conceptualization, TMAS and AHA; methodology, AHA; software, HSA; validation, TMAS, AHA and NKM; formal analysis, TMAS; investigation, TMAS; resources, AHA and NKM; data curation, TMAS; writing—original draft preparation, AHA and NKM; writing—review and editing, TMAS, NKM and HSA; visualization, TMAS; supervision, AHA; project administration, AHA; funding acquisition, not applicable. All authors contributed to editorial changes in the manuscript. All authors read and approved the final manuscript. All authors have participated sufficiently in the work and agreed to be accountable for all aspects of the work.

Conflict of Interest: The authors declare no conflict of interest.

References

1. Sami, W. Physical and magnetic properties of $Ni_{1-x}Cd_xFe_2O_4$ ferrites synthesized by glycine-nitrate auto-combustion process. *Iraqi Journal of Applied Physics* 2024, 20(3), 500.
2. Nawaz, Z.H.; Elhindi, K.M.; Amin, N.; et al. Synthesis and dielectric evaluations of Er doped Mg-Mn-Cr ferrites. *Journal of Ovonic Research* 2024, *20*(6), 793–802. https://doi.org/10.15251/JOR.2024.206.793
3. Salih, S.J.; Mahmood, W.M.; Review on magnetic spinel ferrite (MFe_2O_4) nanoparticles: From synthesis to application. *Heliyon* 2023, 9(6), e16601. https://doi.org/10.1016/j.heliyon.2023.e16601
4. Hossain, S.; Hossain, M.E.; Islam, S.; et al. Synthesis of Sr-doped $Ni_{0.5}Zn_{0.5}Sr_xFe_{2-x}O_4$ and the study of its structural, mechanical, magnetic, and electrical properties for high-frequency applications. *Physics Open* 2023, 17, 100172. https://doi.org/10.1016/j.physo.2023.100172
5. Vedrtnam, A.; Kalauni, K.; Dubey, S.; et al. A comprehensive study on structure, properties, synthesis and characterization of ferrites. *AIMS Materials Science* 2020, *7*(6), 800–835. https://doi.org/10.3934/matersci.2020.6.800
6. Sagayaraj, R.; Aravazhi, S.; Chandrasekaran, G. Review on structural and magnetic properties of (Co–Zn) ferrite nanoparticles. *International Nano Letters* 2021, 11(4), 307–319. https://doi.org/10.1007/s40089-021-00343-z
7. Lisníková, S.; Novák, P.; Kopp, J. Nickel–iron and zinc–iron bimetal oxalates: preparation, characterization and thermal decomposition to spinel ferrites. *Chemical Papers* 2024, 78(1), 1–12. https://doi.org/10.1007/s11696-023-03047-0
8. Kadhim, S.A.; Al-Saadi, T.M. Study of the effect of Ce^{3+} on the gas sensitivity and magnetic properties of $Cu_xCe_{0.3-x}Ni_{0.7}Fe_2O_4$ ferrite nanoparticles. *Materials Science Forum* 2023, 1083, 3–12. https://doi.org/10.4028/p-tw92h3
9. Perveen, S.; Irfan, M.; Jamil, A.; et al. Energy band gap tuning of Co-Zn cubic ferrite by Sm^{3+} ion substitution ($0.00 \leq x \leq 0.075$) to improve spectral, structural, optical and dielectric properties. *Ceramics International* 2025, 51(16), 21354–21376. https://doi.org/10.1016/j.ceramint.2025.02.296
10. Gabal, M.A.; Al Angari, Y.M.; Al-Agel, F.A. Synthesis, characterization and magnetic properties of Cr-substituted Co–Zn ferrites nanopowders. *Journal of Molecular Structure* 2013, 1035, 341–347. https://doi.org/10.1016/j.molstruc.2012.10.061
11. Mahdi, H.I.; Al-Saadi, T.M.; Bakr, N.A. Fabrication and characterization of $Co_xMn_{0.25-x}Mg_{0.75}Fe_2O_4$ nanoparticles for H_2S sensing applications. *Journal of Materials Science: Materials in Electronics* 2023, 34(22), 1634. https://doi.org/10.1007/s10854-023-11064-8
12. Mazen, S.; Abu-Elsaad, N.I.; Nawara, A.S. The influence of various divalent metal ions (Mn^{2+}, Co^{2+}, and Cu^{2+}) substitution on the structural and magnetic properties of nickel–zinc spinel ferrite. *Physics of the Solid State* 2020, 62(7), 1183–1194. https://doi.org/10.1134/S106378342007015X
13. Kane, S.N.; Tiwari, P.; Deepti; et al. Study of structural, magnetic properties and bandgap of spinel $Co_{1-x}Fe_{2+x}O_4$ ferrite. *Materials Today: Proceedings* 2020, 32, 358–364. https://doi.org/10.1016/j.matpr.2020.02.036
14. Khoreem, S.H.; Al-Hammadi, A.H. Enhancing optical properties of Ba-Ni ferrite through nonmagnetic ion doping for sustainable green technologies and renewable energy applications. *Discover Sustainability* 2024, 5(1), 354. https://doi.org/10.1007/s43621-024-00559-x
15. Satti, O.T.; Ghazanfar, U.; Wahab, H.; et al. Tuning optical and dielectric properties of strontium-zinc ferrite nanomaterials through structure-cation engineering. *Scientific Reports* 2025. https://doi.org/10.1038/s41598-025-29798-2
16. Melegy, A.A.; Abdel-Monem, Y.K.; Ali, F.A.; et al. Superparamagnetic Fe_3O_4/ZnO/$ZnFe_2O_4$ nanocomposites for efficient photocatalytic degradation of methylene blue from water under UV light. *Scientific Reports* 2025, 15(1), 40393. https://doi.org/10.1038/s41598-025-24533-3
17. Manohar, A.; Krishnamoorthi, C.; Naidu, K.C.B.; et al. Dielectric, magnetic hyperthermia, and photocatalytic properties of $ZnFe_2O_4$ nanoparticles synthesized by solvothermal reflux method. *Applied Physics A* 2019, 125(7), 477. https://doi.org/10.1007/s00339-019-2760-0

18. El-Fadl, A.A.; Hassan, A.M.; Kassem, M.A. Tunable cationic distribution and structure-related magnetic and optical properties by Cr^{3+} substitution for Zn^{2+} in nanocrystalline Ni-Zn ferrites. *Results in Physics* 2021, 28, 104622. https://doi.org/10.1016/j.rinp.2021.104622
19. Cheema, H.; Yadav, V.; Maurya, R.S.; et al. Structural, optical and electrical properties of Mn-doped $ZnFe_2O_4$ synthesized using sol–gel method. *Journal of Materials Science: Materials in Electronics* 2021, 32(18), 23578–23600. https://doi.org/10.1007/s10854-021-06847-w
20. Ahmed, M.A.; Rady, K.E.S.; El-Shokrofy, K.M.; et al. The influence of Zn^{2+} ions substitution on the microstructure and transport properties of Mn–Zn nanoferrites. *Materials Sciences and Applications* 2014, 5, 932–942. http://dx.doi.org/10.4236/msa.2014.513095
21. Tehranian, P.; Shokuhfar, A.; Bakhshi, H. Tuning the magnetic properties of $ZnFe_2O_4$ nanoparticles through partial doping and annealing. *Journal of Superconductivity and Novel Magnetism* 2018, 32, 1013–1025. https://doi.org/10.1007/s10948-018-4785-6
22. Al-Saadi, T.M.; Ahmed, O.A.; Khaleel, I.H.; et al. The effect of the doping with cobalt transition metal on the dielectric and structural properties of $Fe_{0.5}Co_xMg_{0.95-x}O$ nanoparticles synthesized by Sol-Gel assisted auto-combustion. *Journal of Physics: Conference Series* 2021, 1879(3), 032117. https://doi.org/10.1088/1742-6596/1879/3/032117
23. Al-Saadi, T.M.; Abed, A.H.; Salih, A.A. Synthesis and characterization of $AlyCu_{0.15}Zn_{0.85-y}Fe_2O_4$ ferrite prepared by the Sol-Gel method. *International Journal of Electrochemical Science* 2018, 13(9), 8295–8302. https://doi.org/10.20964/2018.09.04
24. Mohamed, W.S.; Abu-Dief, A.M. Synthesis, characterization and photo catalysis enhancement of Eu_2O_3-ZnO mixed oxide nanoparticles. *Journal of Physics and Chemistry of Solids* 2018, 116, 375–385. https://doi.org/10.1016/j.jpcs.2018.02.008
25. Abu-Dief, A.M.; Mohamed, W.S. α-Bi_2O_3 nanorods: Synthesis, characterization and UV-photocatalytic activity. *Materials Research Express* 2017, 4, 035039. https://doi.org/10.1088/2053-1591/aa6712
26. Yadav, R.S.; Havlica, J.; Hnatko, M.; et al. Magnetic properties of $Co_{1-x}Zn_xFe_2O_4$ spinel ferrite nanoparticles synthesized by starch-assisted sol–gel autocombustion method and its ball milling. *Journal of Magnetism and Magnetic Materials* 2015, 378, 190–199. https://doi.org/10.1016/j.jmmm.2014.11.027
27. Abed, A.H.; Khodair, Z.T.; Al-Saadi, T.M.; et al. Study the evaluation of Williamson–Hall (W-H) strain distribution in silver nanoparticles prepared by sol-gel method. *AIP Conference Proceedings* 2019, 2123(1), 020019. https://doi.org/10.1063/1.5116946
28. Prabhu, Y.T.; Rao, K.V.; Kumar, V.S.S.; et al. X-ray analysis by Williamson-Hall and size-strain plot methods of ZnO nanoparticles with fuel variation. *World Journal of Nano Science and Engineering* 2014, 4, 21–28. https://doi.org/10.4236/wjnse.2014.41004
29. Maensiri, S.; Masingboon, C.; Boonchom, B.; et al. A simple route to synthesize nikel ferrite ($NiFe_2O_4$) nanoparticles using egg white. *Scripta Materialia* 2007, 56(9), 797–800. https://doi.org/10.1016/j.scriptamat.2006.09.033
30. Hlosta, J.; Hrabovská, K.; Rozbroj, J.; et al. Influence of calcination temperature and particle size distribution on the physical properties of $SrFe_{12}O_{19}$ and $BaFe_{12}O_{19}$ hexaferrite powders. *Scientific Reports* 2024, 14(1), 17564. https://doi.org/10.1038/s41598-024-67994-8
31. Amin, N.; Akhtar, M.; Sabir, M.; et al. Synthesis, structural and optical properties of Zn-substituted Co W-ferrites by coprecipitation method. *Journal of Ovonic Research* 2020, 16(1), 11–19.
32. Jamil, M.T.; Ahmad, J.; Bukhari, S.H.; et al. Effect on structural and optical properties of Zn-substituted cobalt ferrite $CoFe_2O_4$. *Journal of Ovonic Research* 2017, 13(1), 45–53.
33. Kannan Y.B.; Saravanan R.; Srinivasan N.; et al. Sintering effect on structural, magnetic and optical properties of $Ni_{0.5}Zn_{0.5}Fe_2O_4$ ferrite nano particles. *Journal of Magnetism and Magnetic Materials* 2017, 423, 217–225. https://doi.org/10.1016/j.jmmm.2016.09.038
34. Trier, S.H.; Abdali, M.S. The structural, magnetic, and optical properties of $Cu_{1-x}Co_xFe_2O_4$ spinel ferrite and its applications. *Al-Qadisiyah Journal of Pure Science* 2020, 25(3), 1–15. https://doi.org/10.29350/jops.2020.25. 3.1122

35. Arshad, M.; Azam, A.; Ahmed, A.S.; et al. Effect of Co substitution on the structural and optical properties of ZnO nanoparticles synthesized by sol–gel route. *Journal of Alloys and Compounds* 2011, 509(33), 8378–8381. https://doi.org/10.1016/j.jallcom.2011.05.047
36. Xian, F.; Li, X. Effect of Nd doping level on optical and structural properties of ZnO: Nd thin films synthesized by the sol–gel route. *Optics & Laser Technology* 2013, 45, 508–512. https://doi.org/10.1016/j.optlastec.2012.06.002
37. Kannan Nithin, K.V.; Krishnappa, M.R. Synthesis and characterization of cobalt-doped cadmium oxide thin films prepared by sol–gel spin coating method. *Journal of Physics: Conference Series* 2019, 1362(1), 012118. https://doi.org/10.1088/1742-6596/1362/1/012118
38. Mangaiyarkkarasi, J.; Sivaganesh, D.; Sasikumar, S. Impact of cobalt doping on the structural, optical, and electronic characteristics of xCo: NiO crystal lattice. *Transition Metal Chemistry* 2025, 50, 673–685. https://doi.org/10.1007/s11243-025-00648-4
39. Hameed, T.A.; Azab, A.A.; Ibrahim, R.S.; et al. Optimization, structural, optical and magnetic properties of $TiO_2/CoFe_2O_4$ nanocomposites. *Ceramics International* 2022, 48(14), 20418–20425. https://doi.org/10.1016/j.ceramint.2022.03.327
40. Al-Ghamdi, A.A.; Al-Hazmi, F.S.; Memesh, L.S.; et al. Effect of mechanochemical synthesis on the structure, magnetic and optical behavior of $Ni_{1-x}Zn_xFe_2O_4$ spinel ferrites. *Ceramics International* 2017, 43(8), 6192–6200. https://doi.org/10.1016/j.ceramint.2017.02.017
41. Tatarchuk, T.R.; Paliychuk, N.D.; Bououdina, M.; et al. Effect of cobalt substitution on structural, elastic, magnetic and optical properties of zinc ferrite nanoparticles. *Journal of Alloys and Compounds* 2018, 731, 1256–1266. https://doi.org/10.1016/j.jallcom.2017.10.103
42. Gurugubelli, T.R.; Babu, B.; Yoo, K. Structural, optical, and magnetic properties of cobalt-doped $ZnAl_2O_4$ nanosheets prepared by hydrothermal synthesis. *Energies* 2021, 14(10), 2869. https://doi.org/10.3390/en14102869